Addressing Barriers to Efficient Renewable Integration

Grant Number: G00865

Proceedings of IECON, 18-21 Oct 2020

Flexible Power Point Tracking in Cascaded H-Bridge Converter-Based Photovoltaic Systems

Hossein Dehghani Tafti,
Georgios Konstantinou,
John E. Fletcher,
Glen G. Farivar,
Salvador Ceballos,
Josep Pou,
Christopher D. Townsend

Please visit the following websites for more information:

- Project summary: https://arena.gov.au/projects/addressing-barriers-efficient-renewable-integration
- Inverter bench testing: http://pvinverters.ee.unsw.edu.au

Flexible Power Point Tracking in Cascaded H-Bridge Converter-Based Photovoltaic Systems

Hossein Dehghani Tafti[(1, *)], Georgios Konstantinou[(1)], John E. Fletcher[(1)],
Glen G. Farivar[(2)], Salvador Ceballos[(2, 3)], Josep Pou[(2, 4)] and Christopher D. Townsend[(5)]
[(1)]School of Electrical Engineering and Telecommunications, University of New South Wales, Australia
[(2)]Energy Research Institute at NTU (ERI@N), Nanyang Technological University, Singapore
[(3)]Tecnalia, Basque Research and Technology Alliance (BRTA), Derio, Spain
[(4)]School of Electrical and Electronic Engineering, Nanyang Technological University, Singapore
[(5)]Department of Electrical, Electronic & Computer Engineering, University of Western Australia, Australia
[(*)]email: Hossein002@e.ntu.edu.sg

***Abstract*—The frequency response support has been added to the new standards and grid codes for the grid-connected photovoltaic (PV) systems, to retain the reliability and quality of the power system under the high penetration of renewable energy resources. This paper proposes an algorithm for the control of cascaded H-bridge (CHB)-based PV systems to achieve frequency response for them. The required power reference, based on the grid operation condition is distributed among the sub-modules (SMs) of the CHB converter, based on the available power from each SM and operational constraints of the system. The details of the proposed control algorithm are provided, while its effectiveness is evaluated on a 1.5-MW PV simulation setup, connected directly to a 6.6-kV grid.**

***Index Terms*—Active power control, cascaded H-bridge converter, flexible power point tracking, photovoltaic systems.**

I. Introduction

The power system is experiencing a drastic increase in the installation of renewable energy resources. The solar energy has obtained a faster growth compared to other types of renewable energy resources, due to the decrease of the photovoltaic (PV) panel cost and abundant availability of the solar energy in most parts of the world. As shown in Fig. 1, the installed PV capacity was increased by 103 GW in 2018, while it was incremented with an additional capacity of 115 GW in 2019 (more than twice the capacity installed in 2015) [1].

Countries with a significant amount of installed renewable energy resources may face several challenges soon. For instance, if the amount of the generated power from renewable energy resources exceeds the load demand during peak power generation periods, the power system may be overloaded and subsequently, protection devices may be triggered [2], [3]. To ensure the stability and quality of the power system, power system operators regulate new requirements for the connection of PV systems to the grid [4], [5], referring to as grid codes and standards. The aim of these new requirements is to reduce the adverse effects of the high penetration of installed PV systems on the power grid.

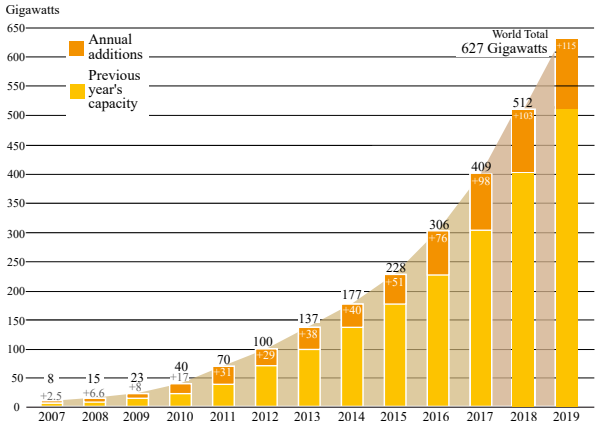

Fig. 1. Solar PV global capacity and annual additions, 2007-2019 [1].

One of these new requirements is the frequency response for PV systems, as illustrated in Fig. 2 for different countries. When the grid frequency is within the frequency control band (f_2 and f_3), a power reserve value of ΔP is considered between the output PV power and the maximum available power (P_{avai}) from the PV system. This enables the PV system to increase its output power to the maximum available value if the grid frequency drops below a certain frequency of f_2. If the frequency is between 47 Hz and f_1, the PV system should inject the maximum power P_{avai} to the grid. On the other hand, for frequencies larger than the upper limit of the frequency band f_3, the PV power reduces based on droop relationship, defined in the standard. When the grid frequency is larger than 52 Hz, the PV system should cease the power generation and disconnect from the grid.

Flexible power point tracking (FPPT) algorithms regulate the PV output power (p_{pv}) to the reference value (p_{fpp}) required by grid codes, as illustrated in Fig. 3 [6]. Several FPPT algorithms are introduced in the literature. Some of these algorithms require extra energy storage, capacitor, etc., to provide flexible power control in PV systems [7], [8]. Other

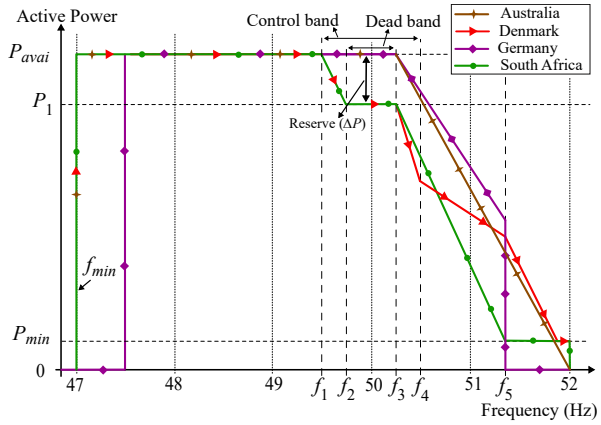

Fig. 2. Frequency support regulations by international grid codes.

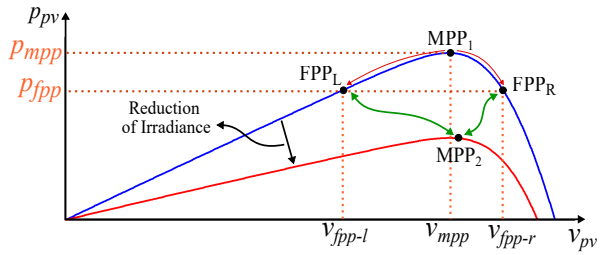

Fig. 3. Flexible power point tracking in PV systems (MPP, maximum power point; FPP, flexible power point).

available FPPT algorithms either modify the voltage controller of the PV system to obtain FPPT [9]–[12] or directly calculate the PV voltage reference corresponding to the PV power reference ($v_{fpp\text{-}l}$ or $v_{fpp\text{-}r}$, as shown in Fig. 3) [13], [14]. The most recent FPPT algorithm with fast dynamic response and low power oscillations at steady-state was introduced in [15]. Although these advanced FPPT algorithms are introduced in the literature, their implementation on multilevel converter-based PV systems, which are the promising solution for medium- and large-scale PV systems, has several challenges, which is not yet studied in the literature.

Among various multilevel converter topologies, the multi-level cascaded H-bridge (CHB) converter, shown in Fig. 4, was introduced as a potential candidate for medium- and large-scale PV systems, because of 1) Reduced semiconductor losses due to the low switching frequency, 2) elimination of the bulky and expensive line-frequency transformer due to the ability of direct connection to medium voltage. The inter-phase and inter-bridge balancing the capacitor voltages in this converter are studied in the literature, while considering the implementation of maximum power point tracking (MPPT) in PV strings [16]–[18].

In order to enable CHB-based PV systems with frequency response requirement of new grid codes, an algorithm for the FPPT operation of these systems is introduced in this paper. The details of the proposed inter-phase and inter-bridge

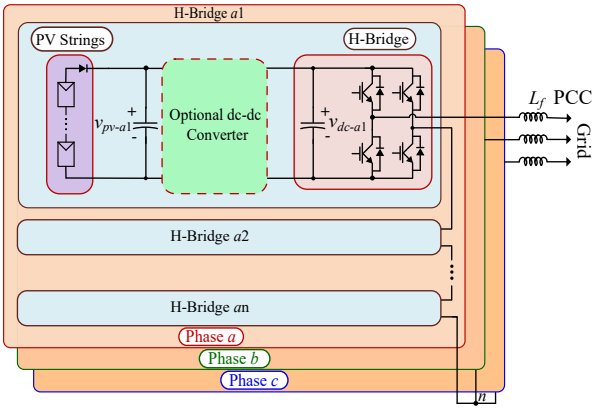

Fig. 4. Circuit topology of the CHB-based PV system.

balancing between the CHB sub-modules (SMs) are provided, while and algorithm to control the dc-dc converters is proposed to obtain FPPT operation. The effectiveness of the proposed algorithm is evaluated on a 1.5-MW PV simulation setup, connected directly to a 6.6-kV grid.

II. Proposed Control Algorithm

The proposed control algorithm for the CHB-based PV system is divided into two parts, and the details are provided in the following subsections:

A. Proposed controller for the CHB Inverter

For the generality of the proposed control algorithm, a N-level CHB inverter is considered in this study. A simplified overview of the proposed control structure of the CHB-based PV system in the $\alpha\beta$-frame is presented in Fig. 5(a). The grid voltages ($v_{pcc\text{-}abc}$ are used to determine the reactive current reference i_q^* requirement according to the grid-codes, while the total energy of dc-links is fed to a proportional-integral (PI) controller to calculate the active current reference i_d^*. The calculated dq-frame current references are then transferred to $\alpha\beta$-frame. The current controller, which is implemented in the $\alpha\beta$-frame, calculates the voltage references based on the error between current references (i_α^* and i_β^*) and instantaneous grid currents (i_α and i_β). The feed-forward filtered voltages from the grid are added to the calculated voltage reference from the current controller to generate the output voltage of the converter.

The controller of the CHB inverter is used to maintain the average capacitor energy ($\overline{E_{dc}}$) by controlling the injected active power into the grid. $\overline{E_{dc}}$ is calculated as follows:

$$\overline{E_{dc}} \triangleq \frac{\sum_{x=a}^{c}\sum_{j=1}^{N} e_{dc-xj}}{N \times 3}, \tag{1}$$

where $x \in \{a,\ b,\ c\}$. The bridge number is denoted by j, while e_{dc-xj} is the capacitor energy of bridge xj, which is calculated as follows:

$$e_{dc} \triangleq \frac{1}{2} \times C_{dc} \times v_{dc-xj}^2, \tag{2}$$

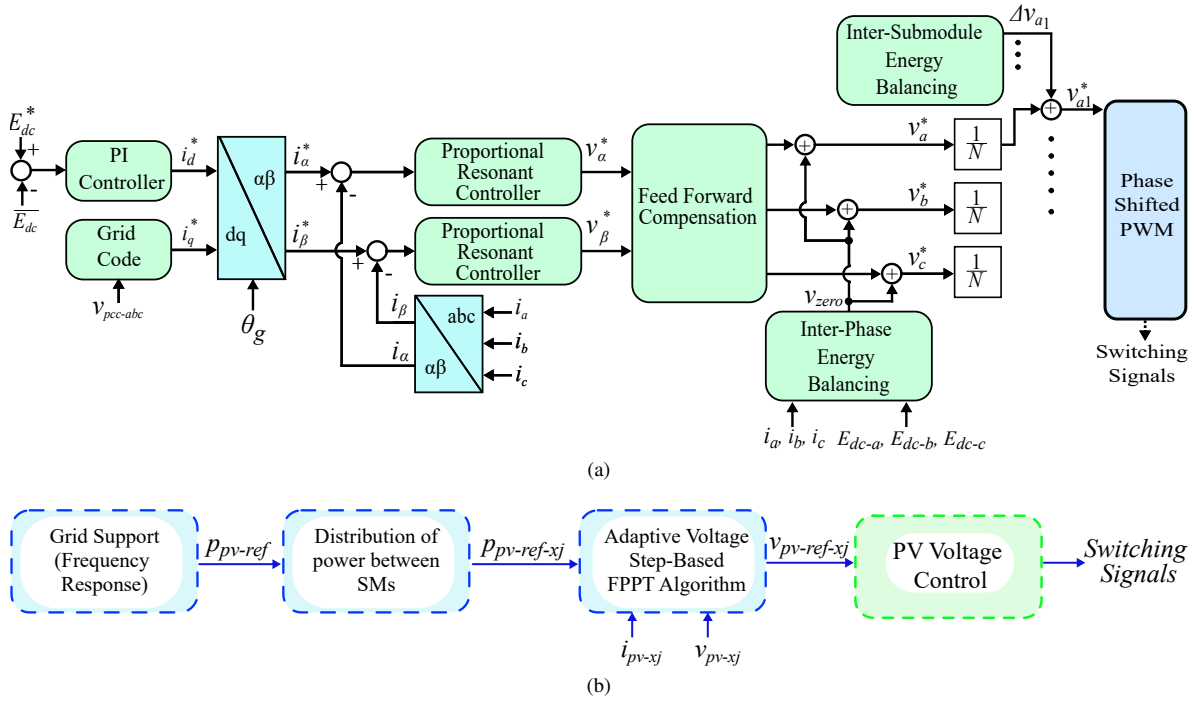

Fig. 5. Proposed control algorithm for the CHB-based PV system: (a) Control algorithm for the CHB inverter and (b) proposed controller for dc-dc converter of each SM.

in which v_{dc-xj} is the capacitor voltage of SM xj, shown in Fig. 4. The capacitor value of each SM is denoted as C_{dc} in this formulation.

As illustrated in Fig. 5, the error between the average energy of all modules $\overline{E_{dc}}$ and module energy reference E^*_{dc} is fed into a PI controller, that calculates the d-axis current reference i^*_d.

The errors between the calculated current references and instantaneous phase currents, transformed to the $\alpha\beta$ coordinate (i_α and i_β), are fed into the proportional resonant (PR) controllers. The calculated $\alpha\beta$ voltage references (v^*_α and v^*_β) are fed into the feed-forward compensation block, which adds the instantaneous grid voltages to the transformed $\alpha\beta$-frame voltage references to the abc-frame. This feature enhances the transient response of the system under grid voltage fluctuations.

Subsequently, an inter-phase energy balancing strategy is applied to balance the average energy between different phases by calculating the required zero-sequence voltage v_{zero} to be added to the three-phase voltage references. Finally, an inter-submodule energy balancing is applied to obtain energy balancing between the SMs of each phase. The details of the inter-phase and inter-submodule energy balancing algorithms can be found in [18].

B. Proposed controller for dc-dc Converters

An overview of the proposed controller for each dc-dc converter of the CHB-based PV system is presented in Fig. 5(b). The grid frequency support block calculates the required power reference $p_{pv\text{-}ref}$ for the system based on the grid frequency and grid requirement, as shown in Fig. 2. While the grid frequency is under normal operation range, a power reserve of ΔP is kept in the PV system to enable the system to respond to grid frequency changes.

The required power reference for the whole PV system is divided proportionally between the SMs, based on their maximum available power and operation limits of each SM

TABLE I
SIMULATION PARAMETERS

Parameter	Value
PV string maximum power, p_{mpp}	100 kW
PV string *MPP* voltage, v_{mpp}	700 V
PV string capacitor, C_{pv}	1 mF
DC-DC converter switching frequency, $f_{s\text{-}dcdc}$	50 kHz
Apparent power, S	1.5 MW
Grid voltage (line-line, rms), $v_{g\text{-}ll}$	6.6 kV
Grid frequency, f	50 Hz
DC-link nominal voltage of each SM, $v_{dc\text{-}xj}$	1.34 kV
DC-link capacitor, C_{dc}	3 mF
Grid connection inductor filter, L_f	9 mH
Carrier frequency of CHB inverter, $f_{carr\text{-}CHB}$	2 kHz
Number of SMs per phase, N	6

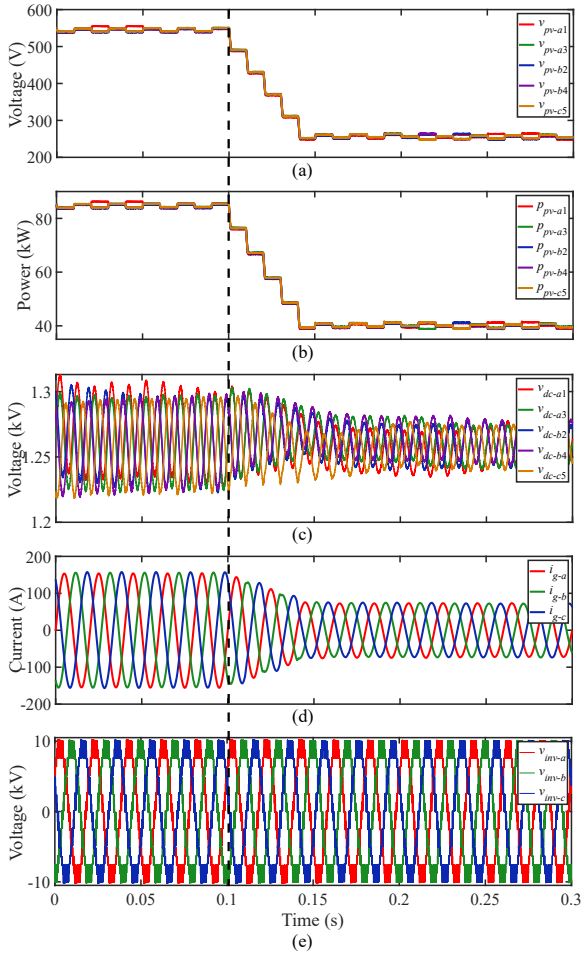

Fig. 6. *Case I*: Performance of the proposed control algorithm under the sudden increase of the grid frequency: (a) PV voltage of selected SMs, (b) PV power of selected SMs, (c) dc-link voltage of selected SMs, (d) inverter output current and (e) inverter output voltage.

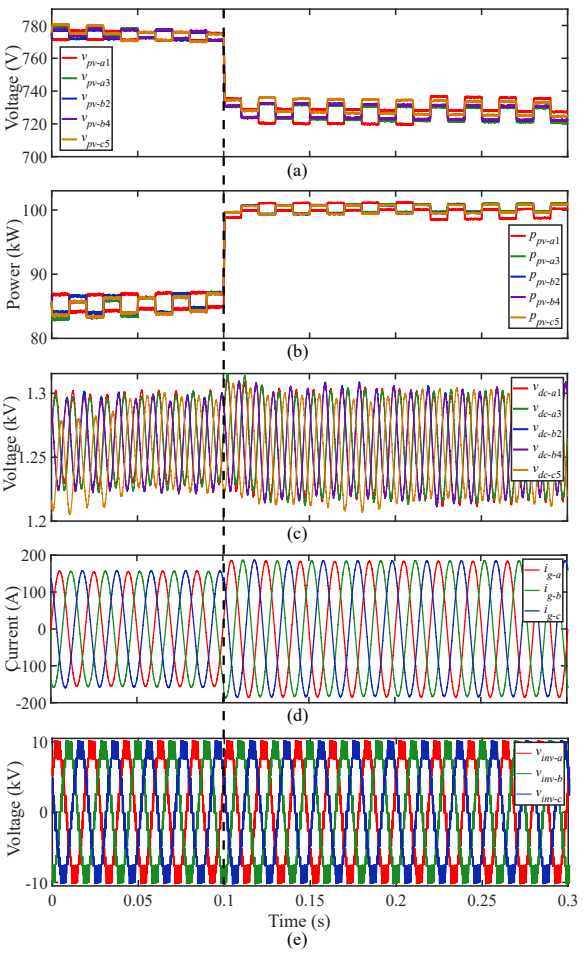

Fig. 7. *Case II*: Performance of the proposed control algorithm under the sudden decrease of the grid frequency: (a) PV voltage of selected SMs, (b) PV power of selected SMs, (c) dc-link voltage of selected SMs, (d) inverter output current and (e) inverter output voltage.

and the operational limit of the CHB inverter. Subsequently, an adaptive voltage-based FPPT algorithm, based on [15] is implemented to calculate the voltage reference of each PV string $v_{pv\text{-}ref\text{-}xj}$. Finally, a conventional voltage controller is implemented to regulate the PV voltage in each SM to its reference value and generate the switching signals. The details of the implemented control strategy can be found in [19].

III. Simulation Results

The effectiveness of the proposed control algorithm to enable the frequency support in CHB-based PV systems is evaluated on a 1.5-MW PV system, directly connected to a 6.6-kV grid simulation setup. The detailed parameters of the system are provided in Table I. Two case studies considering an increase and a decrease in grid frequency are implemented with the following details:

Case I: A sudden increase of the grid frequency is implemented in this case study and results are illustrated in Fig. 6. Based on Fig. 2, during normal frequency interval, before $t = 0.1\,\mathrm{s}$, each dc-dc converter extracts $85\,\mathrm{kW}$ power from the corresponding PV string, to keep $15\,\mathrm{kW}$ power as the reserve in the system. The PV voltage and power of five selected SMs in the systems are shown in Fig. 6(a) and (b). After the detection of an increase in the grid grid frequency at $t = 0.1\,\mathrm{s}$, the proposed control algorithm reduces the power from each PV string from $85\,\mathrm{kW}$ to $40\,\mathrm{kW}$ in less than $0.05\,\mathrm{s}$ by decreasing the PV voltage and moving the operation point to the left-side of the maximum power point (point FPP_L in Fig. 3). It is seen that all the PV strings follow the new power reference. Furthermore, the dc-link voltage of various SMs are balanced under both operating conditions, thank to the implemented inter-phase and inter-submodule energy balancing algorithms. The output current of the inverter, shown in Fig. 6(d), reduces after the detection of the increase in grid frequency, which verifies the reduction of the injected power to the grid. The output voltage of the CHB inverter is also

depicted in 6(e) that shows the multilevel output voltage of the inverter under both operating conditions.

Case II: A sudden decrease of the grid frequency is implemented in this case study and results are illustrated in Fig. 7. In this case study, the output power values of the PV strings are increased to the maximum available power to support the grid in improving the frequency response. It is seen that the capacitor voltages are balanced under all operating conditions and the injected current to the grid increases after the detection of frequency decrease in the grid.

IV. Conclusion

An algorithm for the control of the CHB-based PV system to enable frequency response has been proposed in this paper. The required power reference for the system is distributed between the submodules based on their maximum available power and the operation limits of the converter. Inter-phase and inter-bridge energy balancing algorithms have been implemented to ensure the voltage balancing between all submodules of the system under all operational conditions. The effectiveness of the proposed algorithm has been verified with simulation results. The results show the fast response of the proposed algorithm and its validity for medium- and large-scale PV systems.

V. Acknowledgment

This work was partially supported by the Australian Renewable Energy Agency (ARENA) under the project 'Addressing Barriers to Efficient Renewable Integration', Grant No: G00865, by the Singapore Ministry of Education Academic Research Fund Tier 1 under Grant No: 2019-T1-001-168 (RG 80/19), and by the Basque Country Government under the project 'ENSOL2: Development of Advanced PV Technologies', Grant No: KK-2020/00077.

References

[1] REN21, "Renewables 2019: Global status report (GRS)," 2019. [Online]. Available: http://www.ren21.net/.

[2] Y. Yang, P. Enjeti, F. Blaabjerg, and H. Wang, "Wide-scale adoption of photovoltaic energy: Grid code modifications are explored in the distribution grid," *IEEE Ind. Appl. Mag.*, vol. 21, no. 5, pp. 21–31, Sep. 2015.

[3] Y. Yang, K. A. Kim, F. Blaabjerg, and A. Sangwongwanich, *Advances in Grid-Connected Photovoltaic Power Conversion Systems*. London, UK: Woodhead Publishing, 212 pages, 2018.

[4] *IEEE recommended practice for interconnecting distributed resources with Electric Power Systems Distribution Secondary Networks*, IEEE Std 1547.6 (Revision IEEE Std 1547-2003), Apr. 2018.

[5] Australia/New Zealand Standard AS/NZS 4777.2, "Grid-connected PV systems: Design and installation training manual," Oct. 2015. [Online].Available: https://www.standards.org.au/standardscatalogue/sasnz/electrotechnology/el-042/as-slash-nzs–4777-dot-2-colon-2015.

[6] H. D. Tafti, G. Konstantinou, C. D. Townsend, G. G. Farivar, A. Sangwongwanich, Y. Yang, J. Pou, and F. Blaabjerg, "Extended functionalities of photovoltaic systems with flexible power point tracking: Recent advances," *IEEE Trans. Power Electron.*, vol. 35, pp. 9342–9356, Sep. 2020.

[7] S. Adhikari and F. Li, "Coordinated V-f and P-Q control of solar photovoltaic generators with MPPT and battery storage in microgrids," *IEEE Trans. Smart Grid*, vol. 5, no. 3, pp. 1270–1281, May 2014.

[8] A. Saez-de-Ibarra, A. Milo, H. Gaztanaga, V. Debusschere, and S. Bacha, "Co-optimization of storage system sizing and control strategy for intelligent photovoltaic power plants market integration," *IEEE Trans. Sustain. Energy*, vol. 7, no. 4, pp. 1749–1761, Oct. 2016.

[9] H. D. Tafti, C. D. Townsend, G. Konstantinou, and J. Pou, "A multimode flexible power point tracking algorithm for photovoltaic power plants," *IEEE Trans. Power Electron.*, vol. 34, no. 6, pp. 5038–5042, Jun., 2019.

[10] Y. Yang, F. Blaabjerg, and H. Wang, "Constant power generation of photovoltaic systems considering the distributed grid capacity," in *Proc. of APEC*, pp. 379–385, Mar. 2014.

[11] H. Tafti, A. Maswood, G. Konstantinou, J. Pou, and P. Acuna, "Active/reactive power control of photovoltaic grid-tied inverters with peak current limitation and zero active power oscillation during unbalanced voltage sags," *IET Power Electron.*, vol. 11, no. 6, May 2018.

[12] S. M. Park and S. Y. Park, "Power weakening control of the photovoltaic-battery system for seamless energy transfer in microgrids," in *Proc. of APEC*, pp. 2971–2976, Mar. 2013.

[13] H. D. Tafti, A. I. Maswood, G. Konstantinou, J. Pou, and F. Blaabjerg, "A general constant power generation algorithm for photovoltaic systems," *IEEE Trans. Power Electron.*, vol. 33, no. 5, pp. 4088–4101, May 2018.

[14] R. Gomez-Merchan, S. Vazquez, A. Marquez Alcaide, H. Dehghani Tafti, J. I. Leon, J. Pou, C. A. Rojas, S. Kouro, and L. G. Franquelo, "Binary search-based flexible power point tracking algorithm for photovoltaic systems," *IEEE Trans. Ind. Electron.*, 2020, to be published, doi: 10.1109/TIE.2020.2998743.

[15] H. Dehghani Tafti, A. Sangwongwanich, Y. Yang, J. Pou, G. Konstantinou, and F. Blaabjerg, "An adaptive control scheme for flexible power point tracking in photovoltaic systems," *IEEE Trans. Power Electron.*, vol. 34, pp. 5451–5463, Jun. 2019.

[16] Y. Yu, G. Konstantinou, B. Hredzak, and V. G. Agelidis, "Power balance optimization of cascaded H-bridge multilevel converters for large-scale photovoltaic integration," *IEEE Trans. Power Electron.*, vol. 31, pp. 1108–1120, Feb. 2016.

[17] C. D. Townsend, Y. Yu, G. Konstantinou, and V. G. Agelidis, "Cascaded H-bridge multilevel PV topology for alleviation of per-phase power imbalances and reduction of second harmonic voltage ripple," *IEEE Trans. Power Electron.*, vol. 31, pp. 5574–5586, Aug. 2016.

[18] H. Dehghani Tafti, A. I. Maswood, G. Konstantinou, C. D. Townsend, P. Acuna, and J. Pou, "Flexible control of photovoltaic grid-connected cascaded h-bridge converters during unbalanced voltage sags," *IEEE Trans. Ind. Electron.*, vol. 65, no. 8, pp. 6229–6238, Aug. 2018.

[19] A. Narang, H. Dehghani Tafti, C. D. Townsend, G. Farivar, J. Pou, G. Konstantinou, and S. Vazquez, "An algorithm for fast flexible power point tracking in photovoltaic power plants," in *proc. of IECON*, vol. 1, pp. 4387–4392, Oct. 2019.